



**HAL**  
open science

## AFM tip effect on a thin liquid film

René Ledesma-Alonso, Dominique Legendre, Philippe Tordjeman

► **To cite this version:**

René Ledesma-Alonso, Dominique Legendre, Philippe Tordjeman. AFM tip effect on a thin liquid film. *Langmuir*, 2013, vol. 29, pp. 7749-7757. 10.1021/la4006086 . hal-01020928

**HAL Id: hal-01020928**

**<https://hal.science/hal-01020928>**

Submitted on 8 Jul 2014

**HAL** is a multi-disciplinary open access archive for the deposit and dissemination of scientific research documents, whether they are published or not. The documents may come from teaching and research institutions in France or abroad, or from public or private research centers.

L'archive ouverte pluridisciplinaire **HAL**, est destinée au dépôt et à la diffusion de documents scientifiques de niveau recherche, publiés ou non, émanant des établissements d'enseignement et de recherche français ou étrangers, des laboratoires publics ou privés.



## Open Archive TOULOUSE Archive Ouverte (OATAO)

OATAO is an open access repository that collects the work of Toulouse researchers and makes it freely available over the web where possible.

This is an author-deposited version published in : <http://oatao.univ-toulouse.fr/>  
Eprints ID : 10102

**To link to this article** : DOI:10.1021/la4006086

URL : <http://dx.doi.org/10.1021/la4006086>

**To cite this version** : Ledesma-Alonso, René and Legendre, Dominique and Tordjeman, Philippe *AFM tip effect on a thin liquid film*. (2013) *Langmuir*, vol. 29 (n° 25). pp. 7749-7757. ISSN 0743-7463

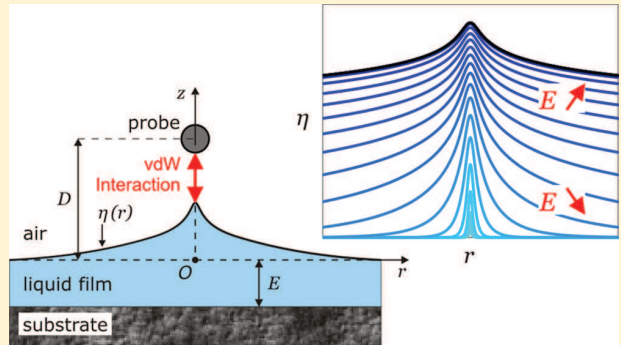
Any correspondance concerning this service should be sent to the repository administrator: [staff-oatao@listes-diff.inp-toulouse.fr](mailto:staff-oatao@listes-diff.inp-toulouse.fr)

# AFM Tip Effect on a Thin Liquid Film

R. Ledesma-Alonso, D. Legendre,\* and Ph. Tordjeman\*

Institut de Mécanique des Fluides de Toulouse (IMFT), INPT-CNRS, Université de Toulouse, Allée du Professeur Camille Soula, 31400 Toulouse, France

**ABSTRACT:** We study the interaction between an AFM probe and a liquid film deposited over a flat substrate. We investigate the effects of the physical and geometrical parameters, with a special focus on the film thickness  $E$ , the probe radius  $R$ , and the distance  $D$  between the probe and the free surface. Deformation profiles have been calculated from the numerical simulations of the Young–Laplace equation by taking into account the probe/liquid and the liquid/substrate interactions, characterized by the Hamaker constants,  $H_{pl}$  and  $H_{ls}$ . We demonstrate that the deformation of a shallow film is determined by a particular characteristic length  $\lambda_F = (2\pi\gamma E^4 / H_{ls})^{1/2}$ , resulting from the balance between the capillary force ( $\gamma$  is the surface tension) and the van der Waals liquid/substrate attraction. For the case of a bulk liquid, the extent of the interface deformation is simply controlled by the capillary length  $\lambda_C = (\gamma / \Delta\rho g)^{1/2}$ . These trends point out two asymptotic regimes, which in turn are bounded by two characteristic film thicknesses  $E_g = (H_{ls} / 2\pi\Delta\rho g)^{1/4}$  and  $E_\gamma = (R^2 H_{ls} / 2\pi\gamma)^{1/4}$ . For  $E > E_g$ , the bulk behavior is recovered, and for  $E < E_\gamma$ , we show the existence of a particular shallow film regime in which a localized tip effect is observed. This tip effect is characterized by the small magnitude of the deformation and an important restriction of its radial extent  $\lambda_F$  localized below the probe. In addition, we have found that the film thickness has a significant effect on the threshold separation distance  $D_{\min}$  below which the irreversible jump-to-contact process occurs:  $D_{\min}$  is probe radius-dependent for the bulk whereas it is film-thickness-dependent for shallow films. These results have an important impact on the optimal AFM scanning conditions.



## 1. INTRODUCTION

The current development of nanotechnology is responsible for the emergence of micro- and nanofluidic systems.<sup>1</sup> A large number of these systems are based on the flow of very thin liquid films in confined geometries.<sup>2</sup> Under these conditions, capillary and van der Waals forces are dominant, and as a consequence, the behavior of liquids is strongly dependent on the film thickness. For instance, the flow relaxation time,<sup>3,4</sup> the slip length,<sup>5</sup> and the glass-transition temperature,<sup>6,7</sup> among other properties, are controlled by the characteristic length of confinement.

The properties of a liquid film as function of its thickness, from the molecular to the macroscopic scale, can be studied by means of atomic force microscopy (AFM) as a result of the recent progress of this technique.<sup>8,9</sup> Indeed, noncontact AFM is a useful method for quantifying the local properties of liquid films,<sup>10</sup> identifying the local positions of interfaces, and detecting liquid-phase domains and studying their rheology. In such experiments, the study of the probe/liquid film interaction is fundamental to understanding the behavior of liquids of different thicknesses. With respect to the extensive work done by means of the surface force apparatus (SFA), we recall that the thickness has been shown to be a fundamental parameter in determining the stability of the film.<sup>11</sup> In addition, it has been proposed, for a liquid nanofilm,<sup>12</sup> that the film

thickness should have a significant effect on AFM measurements and also promising applications.

In our previous studies,<sup>13,14</sup> the surface deformation of a bulk liquid in interaction with an AFM tip has been modeled, solved numerically, and validated with experiments. We have shown that the magnitude of the bulk liquid surface deformation and its curvature are functions of the probe/liquid separation distance. When a probe is approached towards the liquid surface below a threshold separation distance, we have found that the liquid undergoes a jump-to-contact phenomenon, which triggers probe wetting. Knowledge of this critical distance, called  $D_{\min}$ , is essential to determining the experimental optimal conditions for noncontact AFM measurements over liquids. We have demonstrated that a combined approach, based on theory and experiments, leads to a better understanding of the whole phenomenon. In particular, a fine prediction of the Hamaker interaction constant has been deduced from AFM force/distance curves.<sup>13</sup>

The aim of this Article is to analyze the effect of the film thickness on the surface deformation. For this purpose, the Young–Laplace equation has been generalized to include the interaction between the liquid film and the underlying

substrate. The present communication is organized as follows: in section 2, we describe briefly the system configuration, together with the corresponding theoretical model, in which molecular interactions and capillarity are included. Section 3 discusses the general surface deformation and the jump-to-contact phenomenon and their dependency on the involved dimensionless parameters in which some of them are thickness-dependent. Several characteristic length scales, naturally arising in the model, are introduced and employed to describe the surface shape. The theoretical analysis allows us to define two critical film thicknesses, marking the boundaries of a shallow film regime and the bulk behavior, which are presented in section 4 and discussed in section 5. Finally, in section 6 the effects of the probe radius and the film thickness are studied quantitatively in order to apply the results when performing AFM measurements.

## 2. PROBLEM FORMULATION

Consider a stable liquid film of thickness  $E$  deposited over a flat substrate, as shown in Figure 1. When a spherical probe of

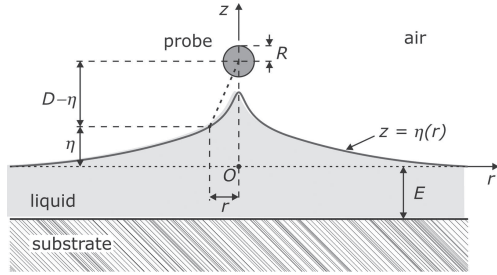


**Figure 1.** Surface deformation of the liquid film interacting with a spherical probe.

radius  $R$  is placed at a distance  $D$  from the liquid free surface, a bump-like shape is observed. Because of the system geometry, the deformation is described by an axisymmetric profile  $z = \eta(r)$ , where  $r$  and  $z$  are the radial and axial coordinates.

On the basis of the Hamaker theory,<sup>15</sup> the attractive interaction potential or pressure field  $\Pi_{pl}$  exerted by the probe over the liquid film is

$$\Pi_{pl} = \frac{4H_{pl}R^3}{3\pi} \frac{1}{[(D-z)^2 + r^2 - R^2]^3} \quad (1)$$

where  $H_{pl}$  is the Hamaker constant of the probe/air/liquid system. Equation 1 is obtained from integrating the London–van der Waals interaction potential of the spherical probe over a differential volume of liquid, anywhere outside the probe. Only the nonretarded interactions are considered in view of the dimensions of common AFM setups.

The presence of the substrate provokes, over the liquid film, the potential field  $\Pi_{ls}$  given by

$$\Pi_{ls} = -\frac{H_{ls}}{6\pi} \left[ \frac{1}{(E+z)^3} - \frac{1}{E^3} \right] \quad (2)$$

where  $H_{ls}$  is the Hamaker constant of the air/liquid/substrate system. This potential is the difference between the so-called disjoining pressure<sup>16</sup> of the initial state and that of the perturbed state (by the approach of the probe). Furthermore, the capillary pressure difference and the hydrostatic pressure

appear in the pressure balance so that the surface shape of the film is described by the generalized Young–Laplace equation

$$\Pi_{pl} - \Delta\rho g\eta = 2\kappa\gamma + \Pi_{ls} \quad (3)$$

where  $\Delta\rho$  is the liquid/air density difference,  $g$  is the gravitational acceleration,  $\gamma$  is the liquid surface tension,  $\eta$  is the local surface position, and  $\kappa$  is the local mean curvature, which, expressed in axisymmetric cylindrical coordinates, takes the form

$$2\kappa = -\frac{1}{r} \frac{d}{dr} \left[ r \frac{d\eta}{dr} \left\{ \left( \frac{d\eta}{dr} \right)^2 + 1 \right\}^{-1/2} \right] \quad (4)$$

Using  $R$  as the characteristic length scale, we introduce dimensionless variables:  $D^* = D/R$  the distance from the center of the probe to the originally undeformed free surface,  $E^* = E/R$  the film relative thickness,  $r^* = r/R$  and  $z^* = z/R$  the horizontal and vertical coordinates; and  $\eta^* = \eta/R$  and  $\kappa^* = \kappa R$ , the interface position and mean curvature. From eqs 1–4, the dimensionless nonlinear ordinary differential equation describing the free surface position results in

$$2\kappa^* - \frac{AH_a}{8}\Pi_{ls}^* + B_o\eta^* - H_a\Pi_{pl}^* = 0 \quad (5)$$

where

$$\Pi_{ls}^* = \frac{1}{(E^* + \eta^*)^3} - \frac{1}{(E^*)^3} \quad (6a)$$

$$\Pi_{pl}^* = \frac{1}{[(D^* - \eta^*)^2 + r^{*2} - 1]^3} \quad (6b)$$

Three dimensionless parameters are present in eq 5: the Hamaker constant ratio  $A = H_{ls}/H_{pl}$ , the modified Hamaker number  $H_a = 4H_{pl}/(3\pi\gamma R^2)$ , and the Bond number  $B_o = \Delta\rho g R^2/\gamma$ .

In AFM setups, the probe radius  $R$  is within the range  $[10^{-9}, 10^{-7}]$  m, and the probe/liquid and liquid/substrate interactions are characterized by Hamaker constants  $H_{pl}$  and  $H_{ls}$  within  $[10^{-21}, 10^{-19}]$  J.<sup>17–20</sup> For air/liquid interfaces, one usually has  $\gamma \in [10^{-2}, 10^{-1}]$  N/m and  $\Delta\rho \in [10^2, 10^4]$  kg/m<sup>3</sup>. Consequently, for a film thickness  $E$  spanning  $[10^{-10}, \infty]$  m, the dimensionless parameters are normally found to satisfy  $A \in [10^{-2}, 10^2]$ ,  $H_a \in [10^{-7}, 10^0]$ , and  $B_o \in [10^{-13}, 10^{-8}]$ .

In particular, considering a PDMS film deposited over a silicon wafer and in interaction with an  $R = 1 \times 10^{-8}$  m silicon AFM probe, the system is characterized by  $\gamma = 3.1 \times 10^{-2}$  N/m,  $\Delta\rho = 9.7 \times 10^2$  kg/m<sup>3</sup>, and  $H_{ls} = H_{pl} = 4 \times 10^{-20}$  J.<sup>13</sup> The nondimensional numbers are then  $A = 1$ ,  $H_a = 5.48 \times 10^{-3}$ , and  $B_o = 3.07 \times 10^{-11}$ , and the film relative thickness should span  $E^* \in [10^{-2}, \infty]$ .

Equation 5 was solved numerically following a previously developed method<sup>14</sup> in which the supplementary term given by eq 6a, arising from the liquid/substrate interaction, has been introduced. The symmetry condition  $[\eta^*]' = 0$  at  $r^* = 0$ , a nearly flat surface profile  $[\eta^*]' \ll 1$ , and a negligible probe/liquid interaction potential  $\Pi_{pl}^* \approx 0$  far from the symmetry axis were maintained as boundary conditions.

To calculate the film deformation analytically, we can write the separation distance  $D^*$  as a function of the apex position  $\eta_0^*$  and the curvature  $\kappa_0^*$  at  $r^* = 0$  as follows

$$D^* = \eta_0^* + \sqrt{1 + [f(\eta_0^*, \kappa_0^*)]^{-1/3}} \quad (7)$$

where the function  $f(\eta_0^*, \kappa_0^*)$  is defined as

$$f(\eta_0^*, \kappa_0^*) = \frac{2\kappa_0^*}{H_a} + \frac{A}{8(E^*)^3} \left[ 1 - \left( 1 + \frac{\eta_0^*}{E^*} \right)^{-3} \right] + \frac{B_o}{H_a} \eta_0^* \quad (8)$$

$D^*$  can also be expressed by introducing  $\varepsilon_0^*$ , the dimensionless gap between the probe surface and the deformed liquid interface inferred from Figure 1:

$$D^* = 1 + \eta_0^* + \varepsilon_0^* \quad (9)$$

In dimensional terms,  $D - R$  represents the gap between the probe and the nondeformed film surface. Comparing eq 9 with an expansion of eq 7 gives

$$\varepsilon_0^* = \frac{1}{2}[f(\eta_0^*, \kappa_0^*)]^{-1/3} - \frac{1}{8}[f(\eta_0^*, \kappa_0^*)]^{-2/3} + O\{[f(\eta_0^*, \kappa_0^*)]^{-1}\} \quad (10)$$

which allows us to calculate the magnitude of the gap if  $f(\eta_0^*, \kappa_0^*)$  is known.

In previous studies,<sup>12–14,21</sup> it has been stated that no solution of the problem can be found for distances below the threshold distance  $D_{\min}^*$  because the jump-to-contact phenomenon takes place. This minimum separation distance also marks the critical point at which the maximum apex deformation  $\eta_{0,\max}^*$  and the maximum curvature  $\kappa_{0,\max}^*$  occur.  $D_{\min}^*$  is obtained directly when  $dD^*/d\eta_0^* = 0$ , which applied to eq 7 gives

$$\frac{1}{36}\{f'(\eta_{0,\max}^*)\}^2 = [f(\eta_{0,\max}^*)]^{8/3}\{1 + [f(\eta_{0,\max}^*)]^{-1/3}\} \quad (11)$$

An expression  $f(\eta_0^*)$ , which must be used in eq 11 to obtain  $\eta_{0,\max}^*$  exists when it is possible to express the curvature in terms of the apex deformation,  $\kappa_0^*(\eta_0^*)$ . Afterward, once  $\eta_{0,\max}^*$  is known,  $D_{\min}^*$  is determined using eq 7.

In the following section, this approach is applied to generate analytical expressions of the maximum deformation  $\eta_{0,\max}^*$  and the minimum distance  $D_{\min}^*$  in the asymptotic cases corresponding to  $E^* \rightarrow 0$  (shallow-film limit) and  $E^* \rightarrow \infty$  (thick-film limit).

### 3. SURFACE SHAPE

**3.1. General Description.** Some typical surface profiles obtained numerically are shown in Figure 2 for a radial extension of about 10 times the probe radius. Note that the

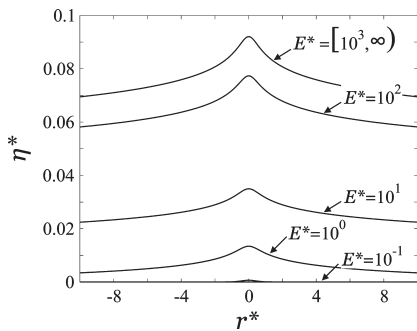


**Figure 2.** Surface profiles of the film  $\eta^*$  obtained from solving eq 5, at a constant  $D^* = 1.29$ , for different values of  $E^*$  and for  $H_a = 5.48 \times 10^{-3}$ ,  $B_o = 3.07 \times 10^{-11}$ , and  $A = 1$ .

presented window is much smaller than the capillary length so that the entire interface deformation is not shown. The profiles are reported for a single separation distance of  $D^* = 1.29$  and for  $H_a = 5.48 \times 10^{-3}$ ,  $B_o = 3.07 \times 10^{-11}$ , and  $A = 1$ . The relative thickness  $E^*$  varies over several orders of magnitude in the range of  $[10^{-10}, \infty]$ . We observe that all of the profiles exhibit a bump-like shape that is roughly parabolic around  $r^* = 0$ , followed by an exponential-like decay. The profiles obtained for  $E^* > 10^2$  are overlapped, indicating the existence of an asymptotic bulk regime. The vertical displacement of the surface weakens in magnitude, and the deformation seems to be confined to a shorter radial extent as  $E^*$  is reduced. In addition, the curvature of the surface at  $r^* = 0$  lowers with decreasing  $E^*$ .

The corresponding behavior of apex deformation  $\eta_0^*$  at  $r^* = 0$  is shown in Figure 3 as a function of the separation distance

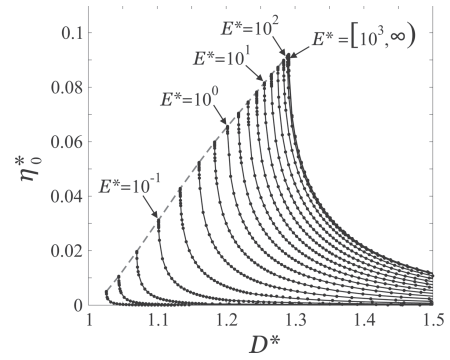


**Figure 3.** Apex position  $\eta_0^*$  of the air/liquid interface as a function of  $D^*$  for different values of  $E^*$  and for  $H_a = 5.48 \times 10^{-3}$ ,  $B_o = 3.07 \times 10^{-11}$ , and  $A = 1$ . (●) Numerical solutions of eq 5 and (---) extreme values  $D_{\min}^*$  and  $\eta_{0,\max}^*$ .

$D^*$ . As observed for infinite film thickness,<sup>14,22</sup> we found a stable and an unstable position of the interface for any film thickness. In Figure 3, we present the stable deformation, corresponding to the minimal free energy of the system, that is present when experiments are performed. Similar hyperbolic evolutions for  $\eta_0^*$  are observed for the different values of  $E^*$ . When sweeping from right to left, as the curve approaches the threshold distance  $D_{\min}^*$ , the slope increases dramatically until a vertical asymptote is reached. At  $D_{\min}^*$ , the maximum possible apex position  $\eta_{0,\max}^*$  is attained. For shorter separation distances, the probe/liquid attraction becomes unconstrained and the so-called jump to contact is observed, which provokes the wetting of the probe in a real situation. Consistent with expectations on physical grounds, a decrease in  $E^*$  leads to a decrease of  $D_{\min}^*$  along with a shrinkage of  $\eta_{0,\max}^*$  as the attractive liquid/substrate potential pulls the liquid film uniformly downward, therefore inhibiting its upward displacement. In other words, when the film thickness is decreased, the jump to contact is shifted to separation distances shorter than that observed for a bulk liquid. Additionally, it is relevant to remark that a reduction of  $E^*$  provokes a similar effect to that induced by a diminution of  $H_a$  for the bulk.<sup>14</sup>

The corresponding evolution of the apex curvature  $\kappa_0^*$  as a function of the surface deformation  $\eta_0^*$  is shown in Figure 4 for different values of the relative thickness  $E^*$ . As a general trend, for a given  $E^*$ , the apex curvature increases along with the associated deformation, showing a nearly constant slope on the presented logarithmic scale. Nevertheless, mainly observed for the curves belonging to  $E^* \leq 10^{-1}$ , the slope gradually becomes

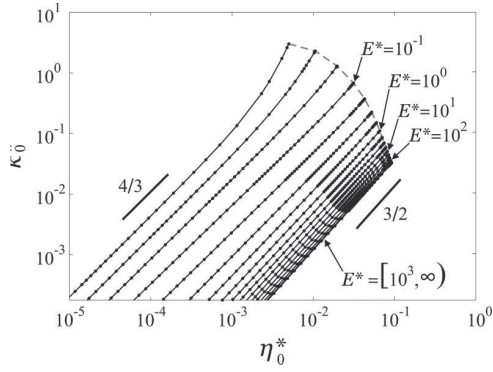


**Figure 4.** Apex mean curvature  $\kappa_0^*$  as a function of  $\eta_0^*$  obtained for different values of  $E^*$  and for  $H_a = 5.48 \times 10^{-3}$ ,  $B_0 = 3.07 \times 10^{-11}$ , and  $A = 1$ . (●) Numerical solution of eq 5 and (---) extreme values  $\kappa_{0,\max}^*$  and  $\eta_{0,\max}^*$ .

steeper as  $\eta_0^*$  increases and approaches the value of  $\eta_{0,\max}^*$ . In most cases, the behavior of each curve seems to be properly described by a power law. For relatively thick films, an exponent of  $3/2$  has been found,<sup>12,13</sup> whereas for shallow films and small deformations an exponent of  $4/3$  is discerned. The theoretical analysis of these two particular power laws is given in section 4.

**3.2. Jump to Contact.** Now the effect of the film thickness on the jump-to-contact condition is discussed. Figure 5 reports the evolution of the maximum apex position  $\eta_{0,\max}^*$  and the minimum separation distance  $D_{\min}^*$  as function of the film relative thickness. Both  $D_{\min}^*$  and  $\eta_{0,\max}^*$  show analogous trends. The bulk behavior is characterized by a plateau, which in the

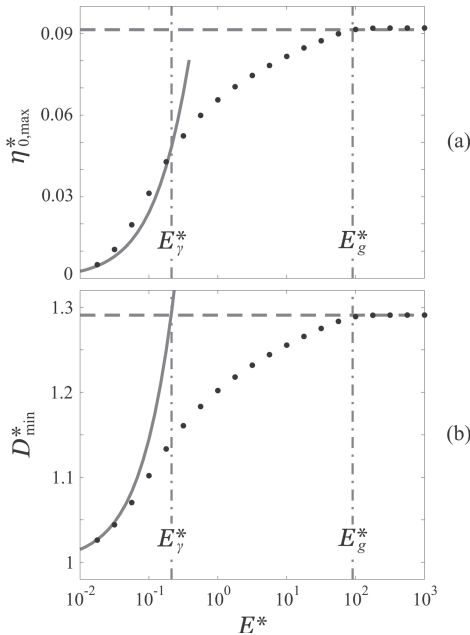


**Figure 5.** (a)  $\eta_{0,\max}^*$  and (b)  $D_{\min}^*$ , as functions of  $E^*$ , for  $H_a = 5.48 \times 10^{-3}$ ,  $B_0 = 3.07 \times 10^{-11}$ , and  $A = 1$ . (●) Numerical solution of eq 5 and asymptotic approximations for (---)  $E^* > E_g^*$  and (---)  $E^* < E_\gamma^*$ , with  $E_g^* = 9.05 \times 10^1$  and  $E_\gamma^* = 2.13 \times 10^{-1}$ . The approximations are obtained by applying eqs 19 and 20 for thick films and eq 23 for shallow films to eqs 11 and 7 in sequence. The characteristic thicknesses,  $E_g^*$  and  $E_\gamma^*$ , are defined in eqs 14 and 15, respectively.

presented case takes the values  $D_{\min}^* \approx 1.29$  and  $\eta_{0,\max}^* \approx 0.09$  for thicknesses  $E^* > 10^2$ . However,  $D_{\min}^* \rightarrow 1$  and  $\eta_{0,\max}^* \rightarrow 0$  when the limit of  $E^* \rightarrow 0$  is approached. These two asymptotic behaviors are associated with two characteristic film thicknesses that will be discussed in more detail in the following section. For intermediate thicknesses typically varying from  $10^{-1}$  to  $10^2$ ,  $D_{\min}^*$  and  $\eta_{0,\max}^*$  go through a transition regime associated with noticeable variations due to the film thickness. It is interesting that for the nondimensional parameters considered here  $\eta_{0,\max}^*$  never takes larger values than the film relative thickness  $E^*$ . In other words,  $\eta_{0,\max}^*/E^* < 1$ .

In Figure 6, interface shape  $\eta^*$  at  $D^* = D_{\min}^*$  is shown as a function of the radial position  $r^*$  for different values of  $E^*$ . As

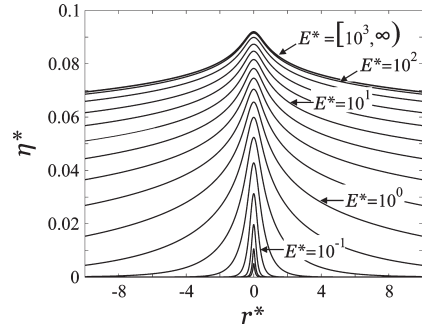


**Figure 6.** Surface profiles of the film  $\eta^*$  obtained from solving eq 5 at  $D^* = D_{\min}^*$  for different values of  $E^*$  and for  $H_a = 5.48 \times 10^{-3}$ ,  $B_0 = 3.07 \times 10^{-11}$ , and  $A = 1$ .

previously discussed, the maximum apex position  $\eta_{0,\max}^*$  and the radial extent of the deformation diminish when  $E^*$  is reduced. As a consequence, the surface profile sharpens, which provokes a dilatation of the curvature at the surface apex. Indeed, as observed in Figure 4, for a fixed value of  $\eta_0^*$ , the apex curvature  $\kappa_0^*$  grows significantly by orders of magnitude when the film relative thickness  $E^*$  decreases.

On the basis of these results, we can define two behaviors depending on the film thickness. For thin films, the amplitude of the surface deformation is small and restricted to a length scale significantly shorter than the capillary length, clearly indicating the appearance of a localized tip effect. This phenomenon is characterized by a deformation profile of confined radial extent, specifically restricted to the near-field underneath the probe. In contrast, for thick films, the surface deformation of large magnitude is observed up to the capillary length. Hence, the tip effect is not observed for thicknesses above a characteristic value, which is found within  $E^* \in [10^2, 10^3]$ , and as a consequence, the deformation corresponds to that of the bulk.<sup>14</sup>

**3.3. Deformation Length Scales.** To understand the localized tip effect and to identify the different length scales arising in this problem, we linearize normalized eq 5 for small surface deformations. Far from the axis, where  $r^* \rightarrow \infty$ , the surface is nearly flat,  $[\eta^*]' \ll 1$ , the probe/liquid interaction potential is negligible,  $\Pi_{pl}^* \approx 0$ , and the liquid/substrate interaction potential,  $\Pi_g^*$ , is approximated by the first-order term in eq 6a for  $[\eta^*] \ll E^*$ . Therefore, the surface profile in this region is obtained from

$$\frac{d^2 \eta^*}{dr^{*2}} + \frac{1}{r^*} \frac{d\eta^*}{dr^*} - [(\lambda_C^*)^{-2} + (\lambda_F^*)^{-2}] \eta^* = 0 \quad (12)$$

where the dimensionless capillary length  $\lambda_C^* = \lambda_C/R = (\gamma/\Delta\rho g R^2)^{1/2}$  and a dimensionless film characteristic length  $\lambda_F^* = \lambda_F/R = (8(E^*)^4/(3AH_a))^{1/2}$  appear.  $\lambda_F = (2\pi\gamma E^3/H_{ls})^{1/2}$  corresponds to the radial distance beyond which the liquid/substrate interaction contributes to the flattening of the liquid surface. A condition for observing the localized tip effect is thus given by  $\lambda_F \ll \lambda_C$ , which is satisfied in the shallow film limit  $E \rightarrow 0$ . As clearly revealed in eq 12, these two length scales are compared through an effective capillary length,  $\lambda_{CF}^* = 1/((\lambda_C^*)^{-2} + (\lambda_F^*)^{-2})^{1/2}$ , that indicates which one of the two mechanisms, gravity or the liquid/substrate interaction, prevails and controls the radial extent of the deformation. In the literature,<sup>12</sup> the inverse of  $\lambda_{CF}^*$  has been introduced as an effective Bond number, which indicates when the effect of the substrate is negligible. Indeed, the exact solution of eq 12 is given by

$$\eta^* = GK_0\left(\frac{r^*}{\lambda_{CF}^*}\right) \quad (13)$$

where  $K_0$  is a zeroth-order modified Bessel function of the second kind and  $G = \eta_{CF}^*/K_0(1)$ , with  $\eta_{CF}^*$  being the surface deformation at  $r^* = \eta_{CF}^*$ . For the studied range of parameters,  $G \lesssim 10^{-2}$  and  $K_0(1) \approx 0.42$ . Thus, for  $r^* \geq \eta_{CF}^*$ ,  $\eta^* \lesssim 10^{-2}$  and  $[\eta^*]' \lesssim 10^{-3}$ , demonstrating the validity of the small deformation hypothesis.

In the particular case of an  $R = 1 \times 10^{-8}$  m silicon AFM probe interacting with a PDMS film of thickness  $E \approx R$  deposited over a silicon wafer, the film characteristic length  $\lambda_F \approx 2.2 \times 10^1 R$  is much smaller than the corresponding capillary length  $\lambda_C \approx 1.8 \times 10^5 R$ .

#### 4. CHARACTERISTIC FILM THICKNESSES

The characteristic radial length scales are now used to highlight the existence of two characteristic film thicknesses. When the capillary length  $\lambda_C$  and the film characteristic length  $\lambda_F$  are of the same order of magnitude, film thickness effects are expected to be observed. The first critical film thickness  $E_g$  is obtained from  $\lambda_F^* \approx \lambda_C^*$

$$E_g \simeq \left(\frac{H_{ls}}{2\pi\Delta\rho g}\right)^{1/4}, \quad E_g^* \simeq \left(\frac{3AH_a}{8B_o}\right)^{1/4} \quad (14)$$

$E_g$  is a constant of the system, independent of the probe radius  $R$ , and  $E_g^* = E_g/R$  depends on dimensionless parameters  $A$ ,  $H_a$ , and  $B_o$ . The value of this critical thickness in common AFM setups is  $E_g \in [10^{-7}, 10^{-6}]$  m, corresponding to  $E_g^* \in [10^0, 10^3]$ .

When the film characteristic length  $\lambda_F$  is on the order of the probe radius, the probe/liquid attraction is opposed only by the liquid/substrate attraction. Hence, from  $\lambda_F^* \approx 1$ , we find a second critical film thickness  $E_\gamma$  that is given by

$$E_\gamma \simeq \left(\frac{R^2 H_{ls}}{2\pi\gamma}\right)^{1/4}, \quad E_\gamma^* \simeq \left(\frac{3AH_a}{8}\right)^{1/4} \quad (15)$$

$E_\gamma$  is a function of the probe radius, scaling as  $R^{1/2}$ , and  $E_\gamma^* = E_\gamma/R$  changes with the product of  $H_a$  and  $A$ . Within common AFM setups, this critical thickness is on the order of  $E_\gamma \in [10^{-10}, 10^{-8}]$  m, corresponding to  $E_\gamma^* \in [10^{-2}, 10^0]$ .

We expect to observe different behaviors depending on the film thickness, relative to the aforementioned critical values. They might be useful for marking the boundaries of the arising

regimes in which the involved mechanisms alternate their contributions.

In Figure 7, the terms in eq 5 are shown as function of the film thickness  $E^*$  under the jump-to-contact condition. The

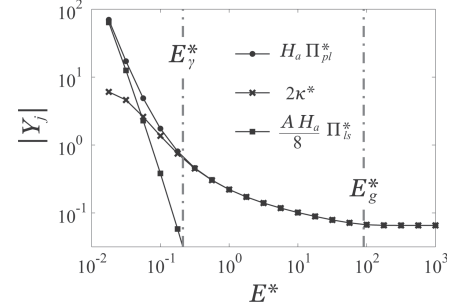


**Figure 7.** Absolute value of the different terms  $Y_j$  from eq 5 for which  $\sum Y_j = 0$  as functions of  $E^*$  at  $D^* = D_{\min}^*$  and for  $A = 1$ ,  $H_a = 5.48 \times 10^{-3}$ , and  $B_o = 3.07 \times 10^{-11}$ . The hydrostatic term  $B_o \eta^*$ , which is not represented herein, remains on the order of  $10^{-11}$ . The critical film thicknesses are  $E_\gamma^* = 2.13 \times 10^{-1}$  and  $E_g^* = 9.05 \times 10^1$ .

presented curves correspond to our reference case for which  $A = 1$ ,  $H_a = 5.48 \times 10^{-3}$ , and  $B_o = 3.07 \times 10^{-11}$ . In addition, hydrostatic term  $B_o \eta^*$  is not shown because its magnitude is very small compared to that of the other terms.

As can be seen on the right-hand side of Figure 7, where  $E^* > E_g^*$ , the curvature and the probe/liquid interaction terms are nearly constant. The presence of the substrate can be disregarded because the liquid/substrate interaction term in eq 5 is negligible. Consequently, the deformation of the liquid surface results from the equilibrium between the surface tension and the probe/liquid interaction, and in dimensionless terms, it is determined only by the values of  $H_a$  and  $B_o$ , as described in previous studies.<sup>14</sup> Moreover, the minimum separation distance  $D_{\min}^*$  and the maximum apex position  $\eta_{0,\max}^*$  do not vary with the film relative thickness  $E^*$ , as depicted in Figure 5. The surface deformation spreads to the effective capillary length, which is essentially given by the usual capillary length  $\lambda_{CF}^* \approx \lambda_C^*$ , because in this case  $\lambda_F^* \gg \lambda_C^*$ . We shall name this regime the asymptotic “thick-film” behavior.

For a film with an intermediate thickness  $E_\gamma^* < E^* < E_g^*$ , though the liquid/substrate term continues to be negligible, the curvature term and the probe/liquid interaction are not constant anymore. These two terms increase slowly and simultaneously, remaining in balance, when reducing the film relative thickness  $E^*$ , as can be discerned from Figure 7. In this case, the deformed surface shape stretches out to the effective capillary length  $\lambda_{CF}^*$ , which takes values between the capillary length  $\lambda_C^*$  and the film characteristic length  $\lambda_F^*$ . This constraint forces the surface to recover from its deformation, getting back to a flat profile at a radial distance shorter than the capillary length. The resulting restrained interface shape shows a curvature that is greater than that of the deformed bulk. Hence, the surface position results from the interplay of the three involved physical mechanisms: surface tension and probe/liquid interaction forces act directly, whereas liquid/substrate interaction force appears by means of an implicit modification of the curvature.

On the left-hand side of Figure 7, where  $E^* < E_\gamma^*$ , the curvature term seems to reach a saturated state. Meanwhile, the probe/liquid and the liquid/substrate attraction terms increase

monotonically, approaching each other in magnitude as  $E^*$  decreases from  $E_g^*$  toward smaller values. Hence, the effect of the proximity of the substrate dominates over that of the surface tension, and the position of the film free surface is retrieved from the equilibrium of the probe/liquid and the liquid/substrate attractive interactions.  $D_{\min}^*$  and  $\eta_{0,\max}^*$  change significantly with the film relative thickness  $E^*$ , as shown in Figure 5. A direct effect of the substrate attraction is observed on the radial span of the surface deformation  $\lambda_{CF}^*$ . In this case,  $\lambda_F^* \ll \lambda_C^*$ ; therefore, the effective capillary length is mainly given by the film characteristic length  $\lambda_{CF}^* \approx \lambda_F^*$ . Hence, the deformation profiles are sharp, and they are restrained to a very narrow zone around  $r^* = 0$ . We name this regime the asymptotic “shallow-film” behavior, where the localized tip effect is observed.

## 5. FILM THICKNESS ASYMPTOTIC BEHAVIORS

**5.1. Thick Film.** Considering the limit of a thick film  $E^* > E_g^*$ , the surface deformation is controlled by the capillary force and the probe/liquid interaction. The force due to the surface deformation can be taken as

$$F_\gamma \approx \pi\gamma R\eta_0^* \quad (16)$$

Also, the force mutually exerted between the probe and the liquid surface can also be approximated by the force between a sphere and a flat surface:<sup>17</sup>

$$F_{pl} \approx \frac{H_{pl}}{6R(\epsilon_0^*)^2} \quad (17)$$

Therefore, when the equilibrium between these two forces is attained, the surface deformation is described by

$$\eta_0^* \approx \frac{H_a}{8(\epsilon_0^*)^2} \quad (18)$$

In the limit  $E^* \rightarrow \infty$ , with the dominant term in eq 8 being the one containing the curvature, the function  $f(\eta_0^*, \kappa_0^*)$  is given by

$$f(\eta_0^*, \kappa_0^*) \simeq \frac{2\kappa_0^*}{H_a} \quad (19)$$

which, combined with the first-order approximation of eq 10, results in an expression for  $\epsilon_0^*$  in terms of  $\kappa_0^*$ . Taking this within eq 18, one obtains the power law relation of the curvature in terms of the apex deformation

$$\kappa_0 \simeq C \sqrt{\frac{3\pi\gamma}{2H_{pl}} \left(\frac{\eta_0}{R}\right)^{3/2}}, \quad \kappa_0^* \simeq C \sqrt{\frac{2}{H_a}} (\eta_0^*)^{3/2} \quad (20)$$

which is in agreement with that observed in Figure 4 for large values of  $E^*$  and has been previously found for the bulk.<sup>12,13</sup> For this case, where  $H_a = 5.48 \times 10^{-3}$  and  $B_o = 3.07 \times 10^{-11}$ , coefficient  $C$  takes a value of  $6.37 \times 10^{-2}$ . The employment of eqs 19 and 20 in eqs 11 and 7 allows us to forecast the asymptotic bulk behavior shown in Figure 5.

**5.2. Shallow Film.** We now focus on the particular evolution observed in Figure 4 for shallow films,  $E^* < E_g^*$ , and small deformations. Consequently, according to the relative contributions shown in Figure 7, the first-order surface deformation results from the balance between the probe/liquid and the liquid/substrate interactions. The force due to the liquid/substrate interaction can be taken as

$$F_{ls} \approx \frac{H_{ls}\eta_0^*}{R(E^*)^4} \quad (21)$$

Equilibrium between this expression and the probe/liquid interaction force, given by eq 17, yields

$$\eta_0^* \approx \frac{(E^*)^4}{6A(\epsilon_0^*)^2} \quad (22)$$

Now, the dominant term in eq 8 comes from the liquid/substrate interaction, and the function  $f(\eta_0^*, \kappa_0^*)$  for  $\eta_0^*/E^* \rightarrow 0$  is given by

$$f(\eta_0^*, \kappa_0^*) \simeq \frac{\eta_0^*}{H_a(\lambda_F^*)^2} \quad (23)$$

The asymptotic shallow film behavior is obtained when combining eq 23 with eqs 11 and 7, which is a good approximation of the numerical results displayed in Figure 5. From the first-order approximation of eq 10, we find an expression for  $\epsilon_0^*$  in terms of  $\eta_0^*$ , which when substituted into eq 22 gives

$$\eta_0^* \approx \frac{(E^*)^4}{24A} \quad (24)$$

Moreover, from the balance between the two interaction terms in eq 5

$$-\frac{1}{8}AH_a\Pi_{ls}^* = H_a\Pi_{pl}^* \quad (25)$$

the free surface shape of the thin film is given by

$$\eta^*[(D^* - \eta^*)^2 + r^{*2} - 1]^3 = \frac{8(E^*)^4}{3A} \quad (26)$$

from which, at  $r^* = 0$  and considering  $D^* \gg \eta_0^*$ , we obtain

$$\eta_0^* \simeq \frac{8(E^*)^4}{3A(D^{*2} - 1)^3} \quad (27)$$

Differentiating eq 26 and evaluating at  $r^* = 0$  gives

$$\kappa_0^* \simeq \frac{16(E^*)^4}{A(D^{*2} - 1)^4} \quad (28)$$

Finally, by combining the last two relations in order to eliminate  $D^*$ , we find that

$$\kappa_0 \simeq \sqrt[3]{\frac{H_{ls}}{H_{pl}} \left(3\frac{\eta_0}{E}\right)^{4/3}} \left(\frac{1}{R}\right), \quad \kappa_0^* \simeq \sqrt[3]{A} \left(3\frac{\eta_0^*}{E^*}\right)^{4/3} \quad (29)$$

which is in agreement with the trend observed in Figure 4 for shallow films and small deformations. Within this regime, the minimum separation distance  $D_{\min}^*$  and the maximum apex position  $\eta_{0,\max}^*$  are significantly modified by the film relative thickness  $E^*$ , in contrast to the thick-film case. Note also that the deformation is dependent on the Hamaker constant ratio,  $A$ , but not on the modified Hamaker and Bond numbers.

## 6. PROBE SIZE EFFECT

With the purpose of determining the experimental parameters for AFM measurements, the probe size and the film thickness effects are quantitatively studied. Therefore, the dimensional jump-to-contact threshold is analyzed, considering the constant physical properties of the system. The combined effect of  $H_a$



and  $E^*$  on the deformation for a given value of  $H_{ls} = H_{pl}$  is equivalent to studying the effects of  $R$  and  $E$  on the free surface displacement. The dimensionless representation depicted in Figure 5a corresponds to the evolution of  $\eta_{0,max}^*$  in terms of  $E^*$  for a single value  $H_a = 5.48 \times 10^{-3}$ . As a consequence, it is possible to reconstruct the dimensional dependency of the maximum apex displacement  $\eta_{0,max}$  on the film thickness  $E$ , but only for  $R = R_3 = 10^{-8}$  m with parameters  $\gamma = 3.1 \times 10^{-2}$  N/m and  $H_{pl} = 4 \times 10^{-20}$  J. Additionally, considering the same physical parameters, we solved eq 5 numerically for different values of  $E$  and for  $R_2 = 10^{-6}$  m and  $R_1 = 10^{-4}$  m. In Figure 8,

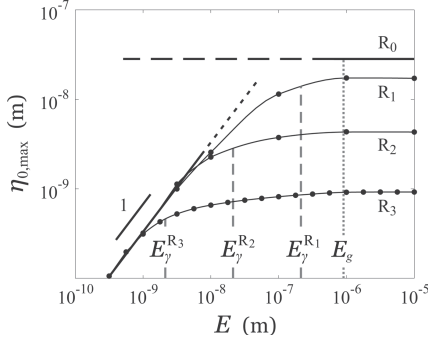


**Figure 8.** Maximum apex displacement  $\eta_{0,max}$  as a function of the film thickness  $E$  for  $H_{ls} = H_{pl} = 4 \times 10^{-20}$  J and different values of the probe radius  $R$  ( $R_1 = 10^{-4}$  m,  $R_2 = 10^{-6}$  m, and  $R_3 = 10^{-8}$  m). The values of  $E_\gamma$ , corresponding to the different values of  $R$ , are summarized in Table 1, as is the value of  $E_g$ . The horizontal line (---) is the solution of eq 11, considering the thick-film approximation given by eqs 19 and 20 for  $R_0 \gtrsim \lambda_C \approx 10^{-3}$  m.

the maximum apex displacement  $\eta_{0,max}$  is displayed as a function of the film thickness  $E$  for the three probe radii. One notes that the evolution of  $\eta_{0,max}(E)$  follows similar tendencies: for  $E < E_\gamma$ ,  $\eta_{0,max}$  increases linearly with  $E$ ; for  $E_\gamma < E < E_g$ ,  $\eta_{0,max}$  grows monotonically as  $E$  increases with a slowly declining slope; and finally for  $E > E_g$ ,  $\eta_{0,max}$  reaches a plateau.

Figure 8 points out that for a shallow film  $E < E_\gamma$  the maximum apex displacement  $\eta_{0,max}$  is independent of the probe radius  $R$ . A linear dependency of the displacement on the thickness,  $\eta_{0,max} = \alpha_0 E$  with  $\alpha_0 \simeq 0.33$ , is found. Because  $E_\gamma$  grows as  $R^{1/2}$ , the linear regime is extended to a larger range of  $E$ . Furthermore, the value of  $\eta_{0,max}$  at the plateau, characteristic of bulk behavior  $E > E_g$ , increases with the value of  $R$ . As depicted in eq 14,  $E_g$  is constant for a given set of physical parameters, whatever the value of  $R$ . In Figure 8, the free surface displacement of a bulk liquid due to its interaction with a probe of millimetric size,  $R_0 = 10^{-3}$  m  $\approx \lambda_C$ , is also represented. In the theoretical case in which  $R = \lambda_C$ , the two critical film thicknesses collapse into a single value,  $E_g = E_\gamma$ . As a

consequence, the value of  $\eta_{0,max}$  obtained with  $R = R_0$  in the bulk regime corresponds to the maximum displacement that the liquid surface can attain by increasing the probe radius, even for  $R > \lambda_C$ . Hence, for probes of larger radius, the system can be modeled as a film interacting with a flat, solid surface for which the maximum apex displacement is approximately the same as for  $R \approx \lambda_C$  and completely independent of  $R$ . Table 1 reports the characteristic parameters computed for the different values of  $R$ .

The combined analysis of Figures 6 and 8 shows that the localized tip effect is observed only for shallow films for which  $E < E_\gamma$ . As a consequence, when  $R$  increases, the localized tip effect is observed at larger thicknesses as a result of the relation between  $E_\gamma$  and  $R$ . Within this regime, the linear dependency of  $\eta_{0,max}$  on  $E$  can be understood by considering that the confined liquid behaves as a linearly elastic solid. This is in agreement with the linear relationship observed between the displacement and the thickness of confined materials undergoing a constant force test.<sup>23</sup> In conclusion, the localized tip effect is characterized by a constant deformation  $\eta_{0,max}/E = \alpha_0$ . In the particular case of  $A = 1$ , the value  $\alpha_0 \approx 0.33$  is found.

A film with a very small thickness compared to the size of the probe ( $R \gg E$ ) corresponds to  $E < E_\gamma$ , so the surface deformation at the jump-to-contact results from the balance between the probe/liquid and the liquid/substrate interactions. Considering the geometric decomposition,  $D_{min} = R + \eta_{0,max} + \varepsilon_{0,min}$ , we can deduce from Figure 5 that the surface displacement and the gap are comparable in magnitude,  $\eta_{0,max} \approx \varepsilon_{0,max}$ . Thus, taking into account the dependency  $\eta_{0,max} = \alpha_0 E$ , we find that the gap is much smaller than the probe radius,  $\varepsilon_{0,min} \ll R$ . Therefore, eq 1 can be condensed to

$$\Pi_{pl} \simeq \frac{H_{pl}}{6\pi(\varepsilon_{0,min})^3} \quad (30)$$

In addition, eq 2 is also reduced to

$$\Pi_{ls} \simeq \frac{\alpha_1 H_{ls}}{6\pi(E)^3} \quad (31)$$

where  $\alpha_1 = 1 - (1 + \alpha_0)^{-3}$ . The balance between these two simplified potentials gives

$$\varepsilon_{0,min} \simeq [\alpha_1 A]^{-1/3} E \quad (32)$$

Using this result, a linear evolution of the gap between the probe surface and the originally flat surface is yielded:

$$D_{min} - R \simeq \{\alpha_0 + [\alpha_1 A]^{-1/3}\} E \quad (33)$$

In Figure 9,  $D_{min} - R$  is shown as a function of  $E$  for different values of  $R$ .  $D_{min} - R$  behaves essentially the same way as  $\eta_{0,max}$  shown in Figure 8. The only difference is that the magnitude of  $D_{min} - R$  is slightly superior to that of  $\eta_{0,max}$  for the same value

**Table 1.** Values of the Dimensionless Parameters, the Characteristic Film Thicknesses, and the Bulk Apex Displacement for the Different Probe Radii and for the Given Physical Properties<sup>a</sup>

$R$	[m]	$R_0 \approx \lambda_C$ ( $10^{-3}$ )	$R_1$ ( $10^{-4}$ )	$R_2$ ( $10^{-6}$ )	$R_3$ ( $10^{-8}$ )
$H_a$	[1]	$5.48 \times 10^{-13}$	$5.48 \times 10^{-11}$	$5.48 \times 10^{-7}$	$5.48 \times 10^{-3}$
$B_o$	[1]	$3.07 \times 10^1$	$3.07 \times 10^3$	$3.07 \times 10^7$	$3.07 \times 10^{11}$
$E_g$	[m]			$9.05 \times 10^{-7}$	
$E_\gamma^R$	[m]	$6.73 \times 10^{-7}$	$2.13 \times 10^{-7}$	$2.13 \times 10^{-8}$	$2.13 \times 10^{-9}$
$\eta_{0,max}$ (bulk)	[m]	$2.83 \times 10^{-8}$	$1.72 \times 10^{-8}$	$4.31 \times 10^{-9}$	$9.18 \times 10^{-10}$

<sup>a</sup> $\gamma = 3.1 \times 10^{-2}$  N/m,  $\Delta\rho = 9.7 \times 10^2$  kg/m<sup>3</sup>, and  $H_{pl} = H_{ls} = 4 \times 10^{-20}$  J.

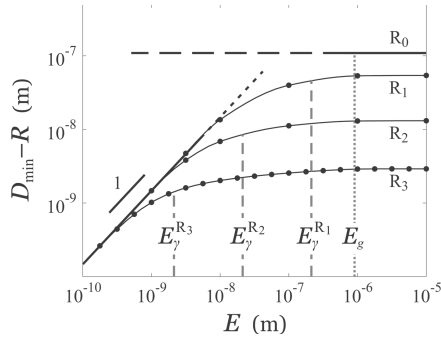


**Figure 9.**  $D_{\min} - R$  as a function of the film thickness  $E$  for  $H_{ls} = H_{pl} = 4 \times 10^{-20}$  J and different values of the probe radius  $R$  ( $R_1 = 10^{-4}$  m,  $R_2 = 10^{-6}$  m, and  $R_3 = 10^{-8}$  m). The values of  $E_\gamma$  corresponding to the different values of  $R$  are summarized in Table 1, as well as the value of  $E_g$ . The horizontal line (---) is the solution of eq 7 for  $D_{\min} - R$ , considering the thick-film approximation already described in Figure 8 for  $R_0 \gtrsim \lambda_C \approx 10^{-3}$  m.

of  $E$ . The linear dependency described by eq 33 is verified in Figure 9 for small values of  $E$ .

The value of gap  $D_{\min} - R$  should be respected when performing AFM measurements because it indicates the experimental set point needed to avoid the jump to contact and the wetting of the probe. For example, colloidal AFM probes, with a radius of  $R = R_2 = 10^{-6}$  m, must be used at a distance of  $D_{\min} - R \gtrsim 10^{-8}$  m when scanning, whereas for common AFM probes with  $R = R_3 = 10^{-8}$  m, we should use  $D_{\min} - R \gtrsim 10^{-9}$  m, which is 1 order of magnitude closer to the interface.

## 7. CONCLUSIONS

We have studied the interaction between an AFM probe and a liquid film deposited over a flat substrate. The competition between probe/liquid and liquid/substrate attraction determines the equilibrium position of the liquid surface. The radial extent of the deformation reaches the effective capillary length  $\lambda_{CF}$ , which takes values between the capillary length  $\lambda_C$  and the film characteristic length  $\lambda_F$ . When the deformation extends up to  $\lambda_{CF} \approx \lambda_C$ , gravity is responsible for the flattening of the surface. However, when  $\lambda_{CF} \approx \lambda_F$ , the liquid/substrate attraction is the mechanism that restrains the deformation.

From these two characteristic length scales, the existence of two characteristic film thicknesses,  $E_\gamma$  and  $E_g$ , is pointed out.  $E_\gamma$  depends on the liquid/substrate interaction constant and the liquid surface tension, also scaling as  $R^{1/2}$ . In contrast,  $E_g$  is independent of the probe radius  $R$ , taking a constant value for a given set of physical properties of the system.

For shallow films (i.e.,  $E < E_\gamma$ ), the maximum apex displacement varies linearly with the film thickness  $\eta_{0,\max} = \alpha_0(A)E$  and is independent of  $R$ . In addition, a localized tip effect is revealed, which is characterized by a deformation of localized radial extent  $\lambda_{CF} \approx \lambda_F$  and small amplitude. For thick films (i.e.,  $E > E_g$ ), no tip effect is observed, and  $\eta_{0,\max}$  takes a fixed value independent of the film thickness  $E$  but given by the probe radius  $R$ .

From a practical point of view with the aim of performing AFM experiments,  $E_\gamma$  emerges as the relevant characteristic thickness, which can be used to separate two regimes: a linear regime for  $E < E_\gamma$  where  $\eta_{0,\max}$  and  $D_{\min}$  are controlled by film thickness  $E$  and a plateau regime for  $E > E_\gamma$  where  $\eta_{0,\max}$  and  $D_{\min}$  are mainly determined by probe radius  $R$ .

## Corresponding Author

\*E-mail: dominique.legendre@imft.fr; philippe.tordjeman@imft.fr. Phone: +(33)0534322858. Fax: +(33)0534322991.

## Notes

The authors declare no competing financial interest.

(1) Bhushan, B., Ed. *Springer Handbook of Nanotechnology*; Springer: New York, 2004.

(2) Bocquet, L.; Charlaix, E. Nanofluidics: from bulk to interfaces. *Chem. Soc. Rev.* **2010**, *39*, 1073–1095.

(3) Li, T.-D.; Riedo, E. Nonlinear viscoelastic dynamics of nanoconfined wetting liquids. *Phys. Rev. Lett.* **2008**, *100*, 106102.

(4) Riedel, C.; Sweeney, R.; Israeloff, N.; Arinero, R.; Schwartz, G.; A., A.; Tordjeman, P.; Colmenero, J. Imagining dielectric relaxation in nanostructured polymers by frequency modulation electrostatic force microscopy. *Appl. Phys. Lett.* **2010**, *96*, 213110.

(5) Maali, A.; Bhushan, B. Measurement of slip length on superhydrophobic surfaces. *Philos. Trans. R. Soc. A* **2012**, *39*, 2304–2320.

(6) Kim, J.; Jang, J.; Zin, W. Estimation of the thickness dependence of the glass transition temperature in various thin polymer films. *Langmuir* **2000**, *16*, 4064–4067.

(7) Grohens, Y.; Hamon, L.; Reiter, G.; Soldera, A.; Holl, Y. Some relevant parameters affecting the glass transition of supported ultrathin polymer films. *Eur. Phys. J. E* **2002**, *8*, 217–224.

(8) Butt, H. J.; Cappella, B.; Kapp, M. Force measurements with the atomic force microscope: technique, interpretation and applications. *Surf. Sci. Rep.* **2005**, *59*, 1–152.

(9) Yacot, A.; Koenders, L. Aspects of scanning force microscope probes and their effects on dimensional measurements. *J. Phys. D: Appl. Phys.* **2008**, *41*, 103001.

(10) Ondarcuhu, T.; Aime, J.-P. *Nanoscale Liquid Interfaces: Wetting, Patterning and Force Microscopy at the Molecular Scale*; Pan Stanford Publishing: Singapore, 2013.

(11) Christenson, H. Capillary condensation due to van der Waals attraction in wet slits. *Phys. Rev. Lett.* **1994**, *73*, 1821–1824.

(12) Quinn, D.; Feng, J.; Stone, H. Analytical model for the deformation of a fluid-fluid interface beneath an AFM probe. *Langmuir* **2013**, *29*, 1427–1434.

(13) Ledesma-Alonso, R.; Legendre, D.; Tordjeman, P. Nanoscale deformation of a liquid surface. *Phys. Rev. Lett.* **2012**, *108*, 106104.

(14) Ledesma-Alonso, R.; Tordjeman, P.; Legendre, D. Multiscale deformation of a liquid surface in interaction with a nanoprobe. *Phys. Rev. E* **2012**, *85*, 061602.

(15) Hamaker, H. C. The London-Van der Waals attraction between spherical particles. *Physica* **1937**, *4*, 1058–1072.

(16) de Gennes, P.-G.; Brochard-Wyart, F.; Quere, D. *Capillarity and Wetting Phenomena: Drops, Bubbles, Pearls, Waves*; Springer: New York, 2004.

(17) Israelachvili, J. N. *Intermolecular and Surface Forces*, 3rd ed.; Academic Press: Burlington, MA, 2011.

(18) Bergstrom, L. Hamaker constants of inorganic materials. *Adv. Colloid Interface Sci.* **1997**, *70*, 125–169.

(19) Visser, J. On Hamaker constants: a comparison between Hamaker constants and Lifshitz-van der Waals constants. *Adv. Colloid Interface Sci.* **1972**, *3*, 331–363.

(20) Mougin, K.; H., H. Wetting of liquid films at nanoscale heterogeneous surfaces. *Europhys. Lett.* **2003**, *61*, 660–666.

(21) Cortat, F. P.; Miklavcic, S. J. How closely can a solid approach an air-water surface without becoming wet? *Phys. Rev. E* **2003**, *68*, 052601.

(22) Wang, Y. Z.; Wang, B.; Xiong, X.; Zhang, J. Spherical solid model system: exact evaluation of the van der Waals interaction between a microscopic or submacroscopic spherical solid and a deformable fluid interface. *Surf. Sci.* **2011**, *605*, 528–538.

(23) Tordjeman, P.; Papon, E.; Villenave, J. Squeeze elastic deformation and contact area of a rubber adhesive. *J. Chem. Phys.* **2000**, *113*, 712–716.